

# Klein collimation by rippled graphene superlattice

M. Pudlak<sup>1</sup> and R.G. Nazmitdinov<sup>2,3,\*</sup>

<sup>1</sup>*Institute of Experimental Physics, 04001 Kosice, Slovakia*

<sup>2</sup>*Bogoliubov Laboratory of Theoretical Physics,*

*Joint Institute for Nuclear Research,*

*141980 Dubna, Moscow region, Russia*

<sup>3</sup>*Dubna State University, 141982 Dubna, Moscow region, Russia*

(Dated: March 3, 2022)

## Abstract

The hybridization of  $\sigma$  and  $\pi$  orbitals of carbon atoms in graphene depends on the surface curvature. Considering a single junction between flat and rippled graphene subsystems, it is found an accumulation of charge in the rippled subsystem due to Klein penetration phenomenon that gives rise to n-p junction. Using this fact, we show that the momentum distribution of electrons in ballistically propagating beam can be selective without a waveguide, or external electric, and/or magnetic fields in graphene strip under experimentally feasible one-dimensional periodic potential. Such a potential is created with the aid of superlattice that consists of periodically repeated graphene pieces with different hybridizations of carbon orbits, produced by variation of the graphene surface curvature. The charge redistribution and selected transmission of electrons, caused by the superlattice, allows to control the electron focusing in the considered system by simply changing the element properties in the superlattice.

---

\*Electronic address: rashid@theor.jinr.ru

## I. INTRODUCTION

There is an enormous experimental and theoretical activity devoted to graphene and graphene based devices. Indeed, a graphene being a zero-gap semiconductor yields exceptionally high mobility of charged carriers. However, the inability to control this mobility in a graphene is a supreme concern of nanoelectronics. Nevertheless, unique properties of graphene nanostructures, discussed below, offer a promising approach in this field.

The low-energy spectrum of graphene is quite well described theoretically in the effective mass approximation by the linear energy dispersion, which is the same as Weyl's equation for massless neutrino [1]. This description has been proved experimentally, for example, by the observation of a relativistic analogue of the integer Hall effect (e.g., [2, 3]). The linear dispersion is explained as a consequence of graphene crystal structure that consists of two equivalent carbon sublattices. This fact allows to introduce graphene quasiparticles with different pseudospin quantum numbers associated with corresponding sublattices. As a result, such quasiparticles are expected to behave differently from those in conventional metals and semiconductors [4]. It was shown in Ref.[5] that the conservation of the pseudospin forbids strictly charged carrier backscattering in a graphene monolayer with electrostatic potential scattering that mimics the n-p junction. The barrier always remains perfectly transparent for the normal incidence of electrons, while the transmission decreases for other angles. By virtue of this fact, electron focusing analogous to optical effects that occur in negative refractive index material is predicted [6]. In fact, it was demonstrated experimentally that: i) turning carrier density in graphene sheet by means of electrical gates [7]; ii) using electrostatic doping from buried gates [8], or iii) transverse magnetic focusing [9], - it is possible to obtain angle-dependent carrier transmission in graphene n-p junction. These results confirm evidently that, indeed, electron transport through graphene n-p junction has much resemblance to light rays crossing a boundary between materials with different optical index. All these phenomena are founded on unimpeded Klein tunneling penetration [10] through gate potential barriers, that is used recently to create a graphene transistor on tunable fermion optics [11].

It is noteworthy to mention that above discussed results are based on assumption of use *external electrical or magnetic* accessories to control the focusing of electron flow. We recall, however, that graphene sheets are not perfectly flat, and ripples are considered as most

natural sources that might be used to control the electron mobility as well. Moreover, by means of the DFT and molecular dynamics simulations it is shown that graphene demonstrates extraordinary stretchability, up to about 20–30%, without being damaged [12]. The amplitude and the orientation of the unidirectional ripples can be controlled with the aid of the applied strain [13]. And further, it is shown that using the hydrogenation it is possible to induce periodic ripples with various thermal conductivity [14].

The effect of the corrugations in graphene on the electronic structure and density of states was evidently demonstrated in Ref.[15]. It is predicted that ripples could create in graphene: i) electron scattering, caused by the change in nearest-neighbor hopping parameters by the curvature [16, 17]; ii) an electrostatic potential [18, 19]; or iii) a chiral transport [20] due to a spin-orbit interaction induced by the surface curvature [21, 22]. Furthermore, one-dimensional (1D) nanoscale periodic ripples could generate a periodic electronic graphene superlattice [23, 24].

Note, that typical transition lengths for n-p junction are less 100 nm (e.g., [7]). A ballistic transport model is sufficient for the study of physics n-p junction devices [25]. It is appropriate at this point to mention a natural way to control the dispersion of the ballistic electron beam in graphene based systems. It was shown in Refs.[26, 27] that the hybridization of  $\pi$  electron orbital of carbon atom depends on the hybridization of  $\sigma$  orbitals. As a matter of fact, the hybridization is different in a flat and a corrugated graphene. The purpose of the present paper is to exploit this fact and suggest the novel n-p junction based on different hybridizations of carbon orbits, produced by variation of the graphene surface curvature. Considering the superlattice that consists of periodically repeated graphene pieces with different hybridizations of carbon orbits, we will demonstrate its high angle-dependent selectivity of the transmitted ballistic electrons. This selectivity allows the electron focusing at low-energy physics of graphene without any additional electrical or magnetic sources, simply by element settings in the superlattice.

## II. THE MECHANISM OF HYBRIDIZATION IN A CURVED GRAPHENE

Let us specify the mechanism of hybridization of  $\pi$  and  $\sigma$  orbitals in the flat and the curved graphene systems. For the sake of discussion, we recapitulate the basic results for the flat graphene in the effective mass approximation (e.g., [28]).

We consider the Hamiltonian for the  $K$  point (similar approach can be applied for  $K'$  point). It depends on two operators  $\hat{k}_x = -i\frac{\partial}{\partial x}$ ,  $\hat{k}_y = -i\frac{\partial}{\partial y}$ , and yields the equation for the envelope function of the flat graphene [28]

$$\begin{pmatrix} \varepsilon_{2p} & \gamma(\hat{k}_x - i\hat{k}_y) \\ \gamma(\hat{k}_x + i\hat{k}_y) & \varepsilon_{2p} \end{pmatrix} \begin{pmatrix} F_A^K \\ F_B^K \end{pmatrix} = E \begin{pmatrix} F_A^K \\ F_B^K \end{pmatrix}. \quad (1)$$

Here, the parameter  $\gamma = \sqrt{3}\gamma_0 a/2$  depends on the length of the primitive translation vector  $a = \sqrt{3}d \simeq 2.46A^\circ$ , with  $d$  being the distance between atoms in the unit cell, and it is assumed that  $\gamma_0 \approx 3$  eV. The energy  $\varepsilon_{2p} = \langle 2p_z | \mathbb{H} | 2p_z \rangle$  is the energy of  $2p_z$ -orbitals of carbon atoms in the flat graphene, directed perpendicular to the graphene surface;  $\mathbb{H}$  is the tight-binding Hamiltonian of the graphene. The solution of Eq. (1) determines the wave function

$$F(x, y) = e^{ik_x x} e^{ik_y y} \frac{1}{\sqrt{2}} \begin{pmatrix} s e^{-i\varphi} \\ 1 \end{pmatrix}, \quad e^{-i\varphi} = (k_x - ik_y) / \sqrt{k_x^2 + k_y^2}, \quad (2)$$

and the energy

$$E = \varepsilon_{2p} + s\gamma \sqrt{k_x^2 + k_y^2}. \quad (3)$$

Here, the sign  $s = -1(+1)$  is associated with the valence (conductance) band. In the flat graphene we have the following hybridization of  $\pi$  and  $\sigma$  orbitals:

$$|\pi\rangle = |2p_z\rangle, \quad (4)$$

$$|\sigma_1\rangle = \frac{1}{\sqrt{3}}|2s\rangle + \sqrt{\frac{2}{3}}|2p_y\rangle, \quad (5)$$

$$|\sigma_2\rangle = \frac{1}{\sqrt{3}}|2s\rangle + \sqrt{\frac{2}{3}} \left( \frac{\sqrt{3}}{2}|2p_x\rangle - \frac{1}{2}|2p_y\rangle \right), \quad (6)$$

$$|\sigma_3\rangle = \frac{1}{\sqrt{3}}|2s\rangle - \sqrt{\frac{2}{3}} \left( \frac{\sqrt{3}}{2}|2p_x\rangle + \frac{1}{2}|2p_y\rangle \right). \quad (7)$$

Let us discuss the hybridization of  $\sigma$  and  $\pi$  orbitals in the graphene with nonzero curvature. The  $\sigma$  orbitals create the bonds between carbon atoms, while the  $\pi$  orbitals determine the electronic properties of the graphene.

For the sake of illustration we consider a zig-zag nanotube (see Fig.1). For the curved graphene (the arc, characterised by the radius  $R$ ) we obtain the space coordinates of the three nearest-neighbor vectors  $\vec{\tau}_i$  in the following form:

$$\vec{\tau}_1 = d(0, 1, 0), \quad (8)$$

$$\vec{\tau}_2 = d\left(\frac{\sqrt{3}}{2} \cos \alpha, -\frac{1}{2}, -\frac{\sqrt{3}}{2} \sin \alpha\right), \quad (9)$$

$$\vec{\tau}_3 = d\left(-\frac{\sqrt{3}}{2} \cos \alpha, -\frac{1}{2}, \frac{\sqrt{3}}{2} \sin \alpha\right), \quad (10)$$

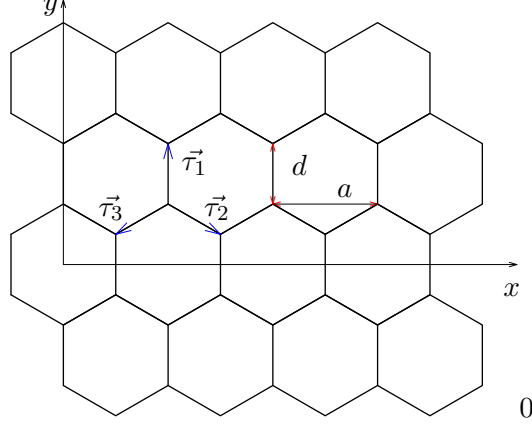


FIG. 1: Graphene lattice. It is assumed that the graphene sheet is wrapped into the tube form with the symmetry axis in the  $y$  direction.

where  $\sin \alpha = a/4R$ . At the limit  $R \rightarrow \infty$ , the vectors  $\vec{\tau}_i$  transform to those of the flat graphene. Evidently, the  $\sigma_i$ -orbitals are determined by the vectors  $\vec{\tau}_i$ . As a result, the  $\sigma_i$  and  $\pi$  orbitals can be expressed as follows

$$|\sigma_1\rangle = c_1|2s\rangle + \sqrt{1 - c_1^2}|2p_y\rangle, \quad (11)$$

$$|\sigma_2\rangle = c_2|2s\rangle + \sqrt{1 - c_2^2} \left( \frac{\sqrt{3}}{2} \cos \alpha |2p_x\rangle - \frac{1}{2} |2p_y\rangle - \frac{\sqrt{3}}{2} \sin \alpha |2p_z\rangle \right), \quad (12)$$

$$|\sigma_3\rangle = c_3|2s\rangle + \sqrt{1 - c_3^2} \left( -\frac{\sqrt{3}}{2} \cos \alpha |2p_x\rangle - \frac{1}{2} |2p_y\rangle - \frac{\sqrt{3}}{2} \sin \alpha |2p_z\rangle \right), \quad (13)$$

$$|\pi\rangle = d_1|2s\rangle + d_2|2p_x\rangle + d_3|2p_y\rangle + d_4|2p_z\rangle. \quad (14)$$

With the aid of the orthonormality conditions  $\langle \sigma_i | \sigma_j \rangle = \delta_{ij}$ ,  $\langle \pi | \sigma_j \rangle = 0$ , and  $\langle \pi | \pi \rangle = 1$ , we determine the parameters  $\{c_k, d_l\}$  and obtain the following expressions for the  $\pi$  and  $\sigma$  orbitals in the lowest order of the ratio  $a/R$ :

$$|\pi\rangle \approx |2p_z\rangle + \frac{a}{2\sqrt{6}R}|2s\rangle + \frac{a}{4\sqrt{3}R}|2p_y\rangle, \quad (15)$$

$$|\sigma_1\rangle = \frac{1}{\sqrt{3}}|2s\rangle + \sqrt{\frac{2}{3}}|2p_y\rangle, \quad (16)$$

$$|\sigma_2\rangle = \frac{1}{\sqrt{3}}|2s\rangle + \sqrt{\frac{2}{3}} \left( \frac{\sqrt{3}}{2}|2p_x\rangle - \frac{1}{2}|2p_y\rangle - \frac{\sqrt{3}a}{8R}|2p_z\rangle \right), \quad (17)$$

$$|\sigma_3\rangle = \frac{1}{\sqrt{3}}|2s\rangle - \sqrt{\frac{2}{3}} \left( \frac{\sqrt{3}}{2}|2p_x\rangle + \frac{1}{2}|2p_y\rangle + \frac{\sqrt{3}a}{8R}|2p_z\rangle \right). \quad (18)$$

The  $\pi$  orbitals are the same for the zig-zag and armchair nanotubes in the lowest order of  $a/R$ . They are used to create the Bloch function in the tight-binding approximation. As a

result, we obtain the following  $\pi$  orbital energy of the curved graphene surface of radius  $R$

$$\begin{aligned}\varepsilon_\pi &= \langle \pi | \mathbf{H} | \pi \rangle = \langle 2p_z | \mathbf{H} | 2p_z \rangle + \frac{1}{24} \left( \frac{a}{R} \right)^2 \langle 2s | \mathbf{H} | 2s \rangle + \frac{1}{48} \left( \frac{a}{R} \right)^2 \langle 2p_y | \mathbf{H} | 2p_y \rangle = \\ &= \varepsilon_{2p} + \alpha \left( \frac{a}{R} \right)^2, \quad \alpha = \frac{1}{24} \langle s | \mathbf{H} | s \rangle + \frac{1}{48} \langle p_y | \mathbf{H} | p_y \rangle.\end{aligned}\quad (19)$$

Note, that the orbitals  $2p_{y,z}$ ,  $2s$  are localized on the same carbon atom and contribute to the  $\pi$  orbital energy [28], while there is no such a contribution from the nondiagonal matrix elements. As a result, we obtain that the energy of the curved graphene consists of the energy of the flat graphene  $\varepsilon_{2p}$ , and the energy of the  $2s$ ,  $2p_y$  orbitals brought about by the curvature (see also [26]).

Using the numerical values for the energies of the  $|s\rangle$  and  $|p_y\rangle$  orbitals of the carbon atom  $\langle s | \mathbf{H} | s \rangle = -12\text{eV}$ ,  $\langle p_y | \mathbf{H} | p_y \rangle = -4\text{eV}$  (e.g., [29]), we obtain for the parameter  $\alpha \simeq -0.58\text{eV}$ . Thus, the energy difference between the  $\pi$  orbitals of the curved and flat graphene is

$$\varepsilon_{2p} - \varepsilon_\pi = \Delta\varepsilon = |\alpha| \left( \frac{a}{R} \right)^2 \approx 0.58 \left( \frac{a}{R} \right)^2 \text{eV}.\quad (20)$$

In the curved graphene the effective mass Hamiltonian, Eq.(1), transforms to the form

$$\hat{H} = \varepsilon_\pi \sigma_0 + \gamma (\hat{k}_x \sigma_x + \hat{k}_y \sigma_y).\quad (21)$$

Here,  $\sigma_x, \sigma_y$  are the Pauli matrices and  $\sigma_0$  is the unity matrix. Solving the Schrödinger equation with the Hamiltonian (45), we obtain the wave function for the curved region

$$F(x, y) = e^{i\kappa_x x} e^{ik_y y} \frac{1}{\sqrt{2}} \begin{pmatrix} s e^{-i\chi} \\ 1 \end{pmatrix}, \quad e^{-i\chi} = (\kappa_x - ik_y) / \sqrt{\kappa_x^2 + k_y^2},\quad (22)$$

with eigenvalue  $E = \varepsilon_\pi + s\gamma\sqrt{\kappa_x^2 + k_y^2}$ .

The difference between  $\varepsilon_\pi$  (curved region) and  $\varepsilon_{2p}$  (flat region) is important when the systems with different surface curvature are coupled. Hereafter, for the sake of simplicity we assume that  $\varepsilon_\pi = 0$ .

### III. THE HYBRID GRAPHENE SYSTEM

#### A. Simple junction

Hereafter, we consider a wide enough graphene sheet  $W \gg M$ , where  $W$  and  $M$  being, respectively, as the width along the  $y$  axis and the length along  $x$  axis of the graphene sheet.

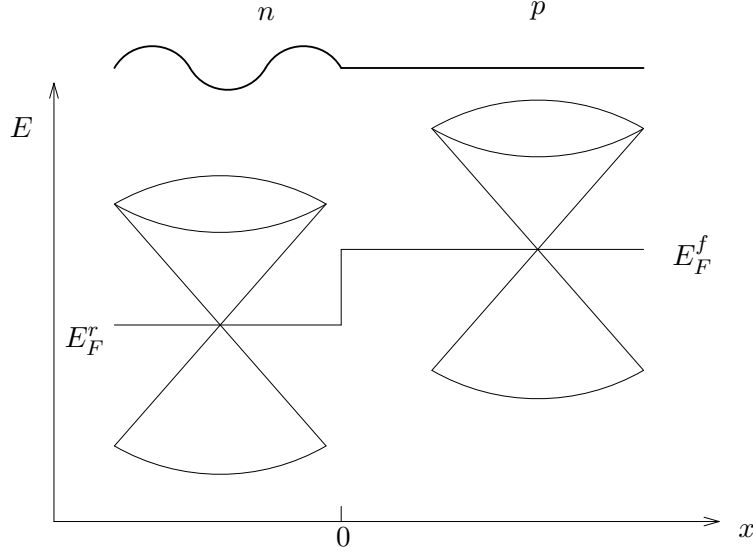


FIG. 2: The sketch of the flat-rippled graphene junction. Here,  $E_F^f$  is the Fermi energy of the flat graphene and  $E_F^r$  is the Fermi energy of the rippled graphene.

It means that we keep the translational invariance along the y axis and neglect the edge effects. Due to different hybridization mechanisms, the Fermi energy of the flat graphene is higher than the Fermi energy of the corrugated graphene (see Sec.II). Let us consider the system (see Fig.2) that consists of the flat graphene piece ( $x > 0$ ) connected to the corrugated graphene piece ( $x \leq 0$ ). In this case the corrugated graphene is modelled by consistently connected arc (with the radius R) and inverted arc (with the same radius) pieces etc. For the sake of convenience, we introduce the notation  $\mathcal{R}(\mathcal{F})$  for a rippled (flat) graphene system.

In the combined system ( $\mathcal{R} + \mathcal{F}$ ) electrons flow from the  $\mathcal{F}$  subsystem to the  $\mathcal{R}$  subsystem. The flow stops once the potential energy difference between two sides of the junction is equal in magnitude and opposite in sign to the difference between two local Fermi levels, similarly to the bimetal interface [30]. The common Fermi level of two subsystems is determined as

$$E_F = \frac{1}{2}(E_F^f + E_F^r) = E_F^r + \frac{|\alpha|}{2} \left(\frac{a}{R}\right)^2. \quad (23)$$

Here, the local Fermi energy of the flat region is  $E_F^f \equiv \varepsilon_{2p}$ , while the local Fermi energy of rippled region is  $E_F^r \equiv \varepsilon_\pi \equiv 0$  (see Sec.II). With the aid of the definition of density of states in the graphene (see Ref.[31])

$$N(E) = g_s \frac{2|E - E_F|}{3\pi\gamma_0^2 a^2} \quad (24)$$

and Eq.(23), we can define the number of electrons moving to the  $\mathcal{R}$  region

$$n = g_s \int_{E_F^r}^{E_F} \frac{2|E - E_F^r|}{3\pi\gamma_0^2 a^2} dE = g_s \int_0^{\frac{|\alpha|}{2} \left(\frac{a}{R}\right)^2} \frac{2EdE}{3\pi\gamma_0^2 a^2} = \frac{1}{3\pi a^2} \left(\frac{\alpha}{\gamma_0}\right)^2 \left(\frac{a}{R}\right)^4. \quad (25)$$

As a result, taking into account the degeneracy value  $g_s = 4$  (spin and valley),  $\gamma_0 = 3\text{eV}$  and  $a = 2.46\text{\AA}$ , the electron density profile in the  $\mathcal{R}$  region, determined by the expression

$$n(R) = 6.6 \times 10^{12} \left(\frac{2.46}{R}\right)^4 \text{cm}^{-2}, \quad (26)$$

yields the density  $n \sim 1.6 \times 10^{12} \text{cm}^{-2}$  at the  $R = 3.5\text{\AA}$ . In other words, there is the extra charge  $\Delta Q = en$  per area in the  $\mathcal{R}$  region and the lack of this charge in the  $\mathcal{F}$  region ( $e$  is the charge of the electron). This situation implies the creation of the n-p junction due to the different hybridization mechanisms. Could we use this fact? The answer on this question is addressed below.

## B. The superlattice effect

Thus, combining two subsystems, we have created a square (sharp) potential step of the height  $V_0 = |\alpha| \left(\frac{a}{R}\right)^2$  on which an electron of energy  $E = E_F > 0$  (Eq.23) is incident. As it was stressed in Ref.[18], in this situation there is an evident analogy with the optical system, when a light beam going through a discontinuity between two transparent media. Evidently, however, that it is quite difficult to arrange experimentally a sharp potential step in graphene based systems. Most likely n-p junction is expected to be atomically smooth (e.g., Ref. [9]).

To model such a situation in our case, we consider the hybrid graphene system that consists of  $\mathcal{R}+\mathcal{S}+\mathcal{F}$  regions. We introduce the notation  $\mathcal{S}$  for the semi-rippled subsystem (see Fig.3) that consists of  $N$  units (superlattice) with the following structure of one unit. It contains the flat and curved (the arc) regions with lengths  $L_1$  and  $L_2$ , respectively. In this case we are faced with the phenomenon of the Klein tunneling (e.g., [18] and references therein) in this hybrid system. To calculate the Klein tunneling through the superlattice ( $\mathcal{S}$  region), we consider the wave function in the rippled region  $[-\infty \leq x < X_1, |y| < W]$  in the form

$$\Psi(x, y) = \left\{ e^{i\kappa_x x} \frac{1}{\sqrt{2}} \begin{pmatrix} e^{-i\chi} \\ 1 \end{pmatrix} + r e^{-i\kappa_x x} \frac{1}{\sqrt{2}} \begin{pmatrix} -e^{i\chi} \\ 1 \end{pmatrix} \right\} e^{ik_y y}. \quad (27)$$



For the first flat sector of the  $\mathcal{S}$  region  $[X_1 \leq x < X_1 + L_1, |y| < W]$  we have

$$\Psi(x, y) = \left\{ \alpha_1 e^{ik_x x} \frac{1}{\sqrt{2}} \begin{pmatrix} -e^{-i\varphi} \\ 1 \end{pmatrix} + \beta_1 e^{-ik_x x} \frac{1}{\sqrt{2}} \begin{pmatrix} e^{i\varphi} \\ 1 \end{pmatrix} \right\} e^{ik_y y}, \quad (28)$$

and for the first rippled sector of the  $\mathcal{S}$  region  $[X_1 + L_1 \leq x < X_1 + L_1 + L_2, |y| < W]$ , we define the wave function in the form

$$\Psi(x, y) = \left\{ \gamma_1 e^{i\kappa_x x} \frac{1}{\sqrt{2}} \begin{pmatrix} e^{-i\chi} \\ 1 \end{pmatrix} + \delta_1 e^{-i\kappa_x x} \frac{1}{\sqrt{2}} \begin{pmatrix} -e^{i\chi} \\ 1 \end{pmatrix} \right\} e^{ik_y y}, \quad (29)$$

and so on. The unknown coefficients  $\alpha_i, \beta_i, \gamma_i, \delta_i$  are obtained from the continuity conditions on the boundary. For the  $\mathcal{F}$  region  $[X_1 + N(L_1 + L_2) \leq x < M, |y| < W]$ , we have

$$\Psi(x, y) = t e^{-ik_x x} \frac{1}{\sqrt{2}} \begin{pmatrix} e^{i\varphi} \\ 1 \end{pmatrix} e^{ik_y y}. \quad (30)$$

We assume that electron moves with the kinetic energy  $E = E_F \equiv V_0/2$ , where the barrier height  $V_0 = |\alpha| \left(\frac{a}{R}\right)^2$ . At this special case  $k_x = \kappa_x = k$ , and, therefore,  $\varphi = \chi$ . Using the continuity conditions on the boundaries, we obtain the following equations for the transmission coefficient  $t$  and reflection coefficient  $r$

$$\begin{pmatrix} 1 \\ r \end{pmatrix} = \begin{pmatrix} A_{11} & A_{12} \\ A_{21} & A_{22} \end{pmatrix}^N D \begin{pmatrix} 0 \\ t \end{pmatrix}, \quad (31)$$

where

$$D = \frac{1}{\cos \varphi} \begin{pmatrix} i \sin \varphi & e^{i\varphi} \\ e^{-i\varphi} & -i \sin \varphi \end{pmatrix}, \quad (32)$$

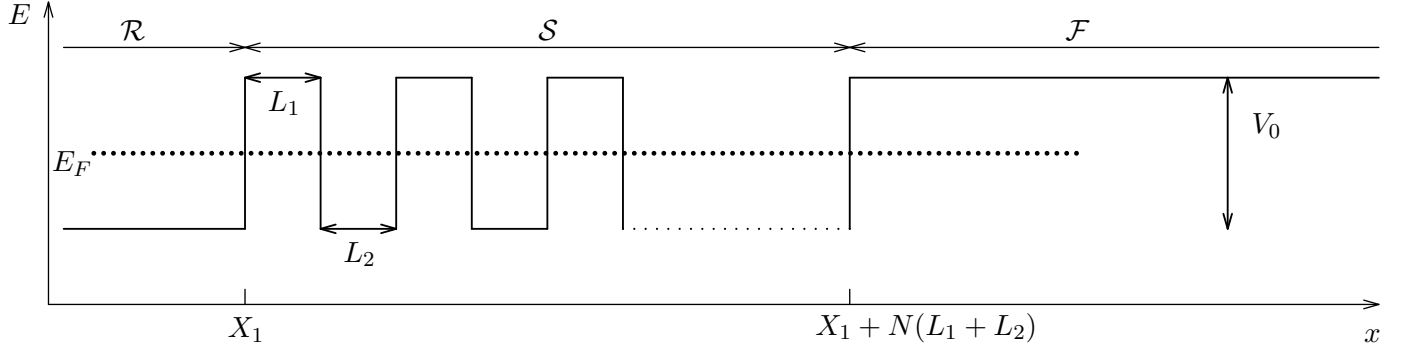


FIG. 3: The hybrid graphene system  $\mathcal{R} + \mathcal{S} + \mathcal{F}$ . The interface ( $\mathcal{S}$ ) is created between  $\mathcal{R}$  and  $\mathcal{F}$  subsystems. The superlattice ( $\mathcal{S}$ ) contains  $N$  units. Each unit consists of the rippled and flat sections. The flat section has length  $L_1$  and the rippled section (arc) has length  $L_2$ .

$$A_{11} = e^{-ikL_2} \left( \cos kL_1 + i \sin kL_1 \frac{1 + \sin^2 \varphi}{\cos^2 \varphi} \right) = A_{22}^*, \quad (33)$$

$$A_{12} = 2e^{i\varphi} e^{ikL_2} \sin kL_1 \frac{\sin \varphi}{\cos^2 \varphi} = A_{21}^*. \quad (34)$$

Taking into account that there is the unitary transformation  $U$  which diagonalizes the matrix  $A$ , i.e.,

$$U^{-1}AU = \begin{pmatrix} \lambda_1 & 0 \\ 0 & \lambda_2 \end{pmatrix}, \quad (35)$$

we can introduce the following notations

$$\begin{pmatrix} A_{11} & A_{12} \\ A_{21} & A_{22} \end{pmatrix}^N = \begin{pmatrix} N_{11} & N_{12} \\ N_{21} & N_{22} \end{pmatrix} \quad (36)$$

with the following elements:

$$N_{11} = \frac{A_{11}(\lambda_1^N - \lambda_2^N) + \lambda_2^{N-1} - \lambda_1^{N-1}}{\lambda_1 - \lambda_2} = N_{22}^*, \quad (37)$$

$$N_{12} = A_{12}A_N = N_{21}^*, \quad A_N = \frac{\lambda_2^N - \lambda_1^N}{\lambda_2 - \lambda_1}. \quad (38)$$

This trick determines the eigenvalues

$$\lambda_{1,2} = a \pm \sqrt{a^2 - 1}, \quad a = (A_{11} + A_{22})/2, \quad (39)$$

$$a = \cos[k(L_1 - L_2)] + 2 \sin(kL_1) \sin(kL_2) \frac{\sin^2 \varphi}{\cos^2 \varphi}. \quad (40)$$

As a result we can calculate analytically the electron transmission probability across the interfaces as

$$T_N(k_y) = |t|^2 = \frac{\cos^2 \varphi}{1 + 4 \frac{\sin^2 \varphi}{\cos^2 \varphi} \sin(kL_1) A_N \Pi}, \quad (41)$$

where

$$\Pi = A_{N-1} \sin(kL_2) + A_N \left( \sin(kL_1) + \sin[k(2L_2 - L_1)] + 4 \frac{\sin(kL_1) \sin^2(kL_2) \sin^2 \varphi}{\cos^2 \varphi} \right), \quad (42)$$

$$\sin^2 \varphi = \frac{k_y^2}{k_F^2}, \quad k = \sqrt{k_F^2 - k_y^2}. \quad (43)$$

If any of the parameters  $L_1$ ,  $L_2$ , or  $N$  are zero, or the condition  $kL_1 = \pi n$ ,  $n = 0, \pm 1, \dots$  is fulfilled, Eq.(41) determines the transmission probability through the sharp step:  $T(k_y) =$

$\cos^2 \varphi$ . Note, that in the n-p junction creating by the ripple-flat graphene system, the Fermi momentum  $k_F$  depends on the ripple radius [see also Eq.(23)]

$$E_F = \gamma k_F \Rightarrow k_F = \frac{|\alpha|}{2\gamma} \left( \frac{a}{R} \right)^2 = 0.46 \left( \frac{a}{R} \right)^2 \text{ nm}^{-1}. \quad (44)$$

Evidently, one is able to control the degree of focusing of the electron beam by fine turning of the angle  $\phi$  with the aid of the discussed parameters and, additionally, by means of the ripple radius as well.

In contrast, for nonzero values of the above parameters, we expect a smooth n-p junction. In order to trace the dependence of the transmission probability on the incident angle of electrons, we calculate numerically Eq.(41) at  $L_1 = L_2 = L$  (see Fig.4). It is noteworthy that the superlattice leads to the selective transmission of electrons. For a small number of  $N$  elements in the  $\mathcal{S}$  subsystem the transmission probability is nonzero for a wide range of

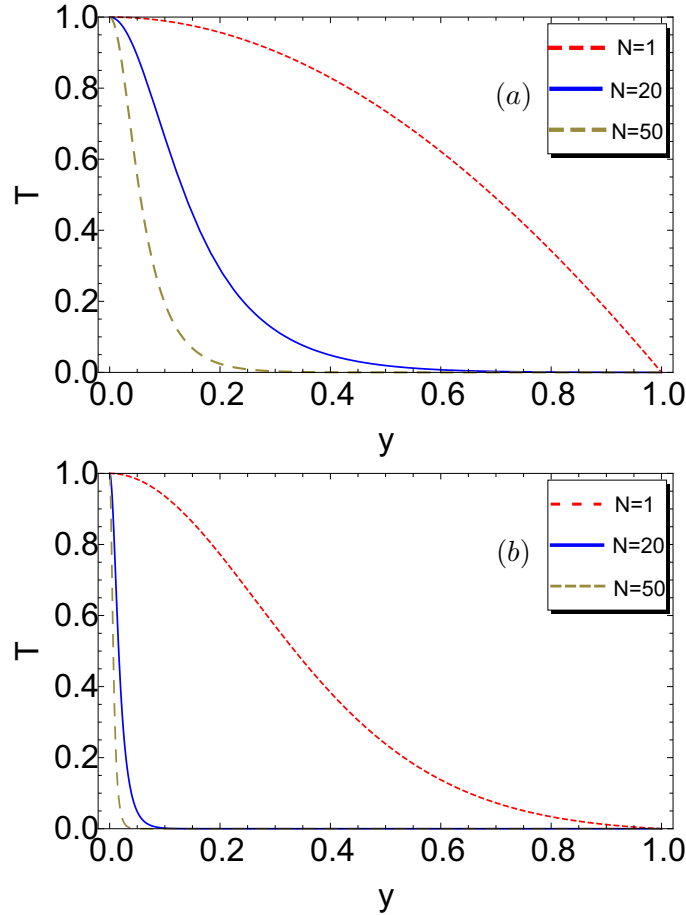


FIG. 4: (Color online) The transmission probability  $T_N$  as a function of the incident direction of the electron flow  $y = k_y/k_F$ : (a)  $k_F L = 0.1$ ; (b)  $k_F L = 1$ .

values of  $k_y$  (see results for  $N = 1, 20$ ). However, the larger the number of  $N$  elements in the superlattice, the stronger the selectivity effect for ballistic electrons. Our system focuses the electronic flow, selecting the transmission of those trajectories that are close to the normal incidence. In fact, for a large enough number  $N$  elements of the superlattice the selection does not depend on the incident direction of an electron flow at all ! Indeed, at  $N \gg 1$ , only for the direction perpendicular to the surface of the  $\mathcal{S}$  subsystem there is almost the ideal transmission, while for the other angles ( $k_y \neq 0$ ) there is the strong backscattering.

To elucidate the advantage/disadvantage of the superlattice effect for ballistic transport we compare the obtained results with those obtained with the aid of the smooth step potential in the region around the n-p junction. We model this by the Hamiltonian in the form

$$\hat{H} = v(x)\sigma_0 + \gamma(\hat{k}_x\sigma_x + \hat{k}_y\sigma_y). \quad (45)$$

Here, the smooth step potential

$$v(x) = \frac{V_0}{2} (1 + \tanh(x/\ell)) \quad (46)$$

is defined in the region  $-\ell \leq x \leq \ell$  (see Fig.5). The transmission probability for the potential (46) is determined by the expression

$$T_{sm}(k_y) = \left[ \sinh \left( \pi k_F \ell \sqrt{1 - \left( \frac{k_y}{k_F} \right)^2} \right) / \sinh \pi k_F \ell \right]^2. \quad (47)$$

Details of calculations could be traced with the aid of Ref.[32]. In our case  $E_F = \gamma k_F \equiv V_0/2$ , and, correspondingly,  $k_F = V_0/2\gamma$ . In the limit  $k_F \ell \ll 1$ , we obtain the transmission probability through the sharp step,  $T(k_y) = \cos^2 \varphi$ . In contrast, at the condition  $k_F \ell \gg 1$  we obtain (see Appendix A)

$$T_{sm}(k_y) \approx \exp(-\pi k_F \ell \sin^2 \varphi), \quad (48)$$

which coincides with the result [5]. Thus, for the potential (46) the range of transmitted angles is controlled by the ratio  $k_F \ell \sim \ell/\lambda_F$ , where for our choice of parameters [see also Eq.(44)]

$$\lambda_F \approx 13.65 \left( \frac{R}{a} \right)^2 nm. \quad (49)$$

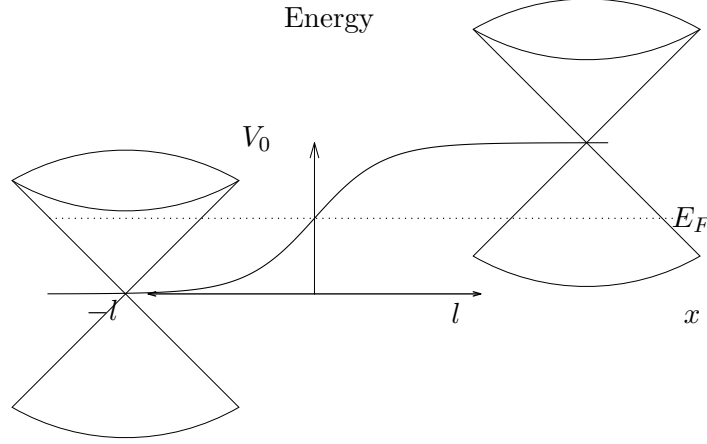


FIG. 5: The sketch of the smooth interface potential.

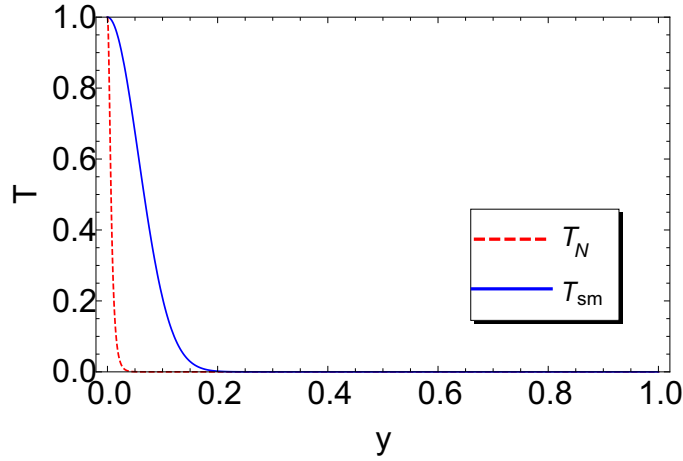


FIG. 6: (Color online) The transmission probabilities  $T$  as a function  $y = k_y/k_F$ : dashed line connects the results for  $N = 50$  elements ( $T_N$ ) at  $k_F L = 1$ ; solid line connects the results for the smooth potential ( $T_{sm}$ ) at  $k_F \ell = 50$ .

The superlattice, that consists of 50 units, produces the selectivity that is much stronger than the one of the smooth potential step (see Fig.6). In the both cases the length of the interface is  $100/k_F$ .

Before to finalize this section there are a few comments in order. Note that our results are valid for both  $K$  and  $K'$  valleys. The basic difference between the corresponding Hamiltonians consists in the sign of the momentum  $k_y$  (see for details [21]). While in our model the results depend on  $k_y^2$  form, and, correspondingly, our conclusions are valid for  $K$  and  $K'$  valleys. We recall that the translational invariance along the  $y$  axis is kept in our model, while the edge effects are neglected. Therefore, the average current is defined as  $\mathbf{j} = s\mathbf{k}/k$

(see also Sec.2.4 in Ref.[18]), where  $s = \text{sign}(E_{kin})[E_{kin} \equiv s\gamma\sqrt{k_x^2 + k_y^2}]$ .

This is true only if one neglects the dependence of the hopping integrals between  $\pi$  orbitals in zig-zag or armchair graphene surface curvatures. In order to illuminate the effect of this dependence on two interfaces, we have to calculate the shift in the origin of  $k_{x,y}$  by  $\Delta k_{x,y}$ , produced by terms of the order of  $(a/R)^2$  neglected in our consideration. In our analysis we follow the arguments discussed by Ando (see §5 in [21]). In the effective mass approximation for the zig-zag interface we obtain

$$\Delta k_x = \mp \frac{a}{4\sqrt{3}R^2} \left( 1 - \frac{3}{8} \frac{\gamma'}{\gamma} \right), \quad (50)$$

$$\Delta k_y = 0, \quad (51)$$

where the upper sign corresponds to the  $K$  point, while the lower sign to the  $K'$  point. The parameter  $\gamma = \sqrt{3}\gamma_0 a/2 = -\sqrt{3}V_{pp}^\pi a/2$ ,  $\gamma' = \sqrt{3}(V_{pp}^\sigma - V_{pp}^\pi)a/2$ , where  $V_{pp}^\pi$  and  $V_{pp}^\sigma$  are the hopping integrals for  $\pi$  and  $\sigma$  orbitals,  $a$  is the length of the primitive translation vector. We recall that in our model it is assumed that  $V_{pp}^\pi \approx -3$  eV and  $V_{pp}^\sigma \approx 5$  eV. Therefore, we have  $\gamma'/\gamma \approx 8/3$ , i.e.,  $\Delta k_x \approx 0$ . Thus, in the case of zig-zag interface the shifts are negligibly small, i.e.,  $\Delta k_x \approx 0$ ,  $\Delta k_y = 0$ . We conclude that the symmetry between  $K$  and  $K'$  valleys is conserved, Q.E.D.

In the case of the armchair interface we obtain that

$$\Delta k_x = 0, \quad (52)$$

$$\Delta k_y = \mp \frac{a}{4\sqrt{3}R^2} \left( \frac{5}{8} \frac{\gamma'}{\gamma} - 1 \right). \quad (53)$$

In other words,  $\Delta k_x = 0$ ,  $\Delta k_y \neq 0$ . In this case this curvature dependence breaks the symmetry between  $K$  and  $K'$  valleys. The analysis of the effects related to this symmetry breaking requires the separate studies and is beyond the scope of the present paper.

### C. Conductance

From the transmission probability, the conductance is given by the Landauer formula

$$G_N = 4 \frac{e^2}{h} \int_{-k_F}^{k_F} T_N(k_y) \frac{dk_y}{2\pi/W} = 4 \frac{e^2}{h} \frac{k_F W}{\pi} I_N. \quad (54)$$

Here, the integral  $I_N$ , defined by the expression

$$I_N = \int_0^1 T_N(u) du, \quad u = \frac{k_y}{k_F}, \quad (55)$$

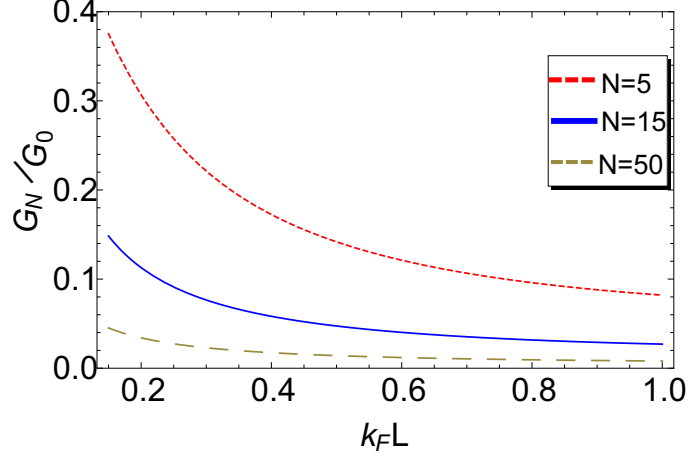


FIG. 7: (Color online) The relative conductance  $G_N/G_o$  as a function of the dimensionless parameter  $k_F L$  for various values of  $N$  units in super-lattice section.

characterizes the efficiency of the selection. For example, at  $L_1 = L_2 = L$  and  $k_F L \approx 1$ , we obtain for  $N = 1, 2$ :

$$I_1 = \int_0^1 \frac{1 - u^2}{(1 + 4(k_F L)^2 u^2)^2} du = 0.33 \quad (56)$$

and

$$I_2 = \int_0^1 \frac{1 - u^2}{(1 + [16(k_F L)^4 + 12(k_F L)^2] u^2)^2} du = 0.14 \quad (57)$$

For the perfect transmission, i.e., for  $T(k_y) = 1$  the conductance

$$G_o = 4 \frac{e^2}{h} \int_{-k_F}^{k_F} \frac{dk_y}{2\pi/W} = 4 \frac{e^2}{\pi h} k_F W \quad (58)$$

is the natural unit, since  $G_N = G_o I_N$ .

The selective electrons transmission across the interface created by  $N$  units is demonstrated on Fig.7, where the dependance of  $G_N/G_o$  on the dimensionless parameter  $k_F L$  is depicted. The electron conductivity  $G_N$  across the interface with  $N$  units is much smaller in comparison to  $G_o$  for enough large  $N$ .

We recall that the estimation for the smooth step yields the value [5, 18]

$$G_{sm} = 2 \frac{e^2}{\pi h} W \sqrt{\frac{k_F}{l}} = \frac{G_o}{2\sqrt{k_F \ell}}, \quad (59)$$

that describes the selectivity effect at the condition  $k_F \ell \gg 1$ .

In order to achieve the smooth step effect, the corrugations with gradually increasing curvature can be used in our case. This conditions leads to the inequality

$$G_{sm} > G_N \Rightarrow \sqrt{2\pi \ell / \lambda_F} \times I_N < 1/2. \quad (60)$$

If we hold fixed the condition  $\ell = NL$ , this inequality determines the number of elements  $N$  and their length  $L$  at the same length  $\ell$  for the smooth potential and the superlattice. Thus, by appropriate choice of the product  $NL$  one can always use the advantage of electron flow focusing through the superlattice, which number of elements can be controlled externally. Moreover, one can use additionally the fine turning of the ripple radius and change carrier charge densities on different sides of our hybrid system.

#### IV. SUMMARY

Based on the fact of the different type of hybridization of carbon atom orbitals in the flat and the corrugated graphene pieces, we developed the model of n-p junction. The  $\pi$  orbital dependence on the surface curvature means that the local chemical potential varies with the curvature. In the approximation of the effective mass Hamiltonian, this fact corresponds to the effective electric field that depends on the electron position. This effect becomes important once it would be possible to create a graphene system with controlled variation of the surface curvature. In fact, there are a few experimental techniques that demonstrate evidently a spatial variation in graphene sheets nowadays. For example, the electrostatic manipulation allows to form ripples without any change of doping [33]. Another approach is based on the chemical vapor deposition that provides quite promising way to create periodic nanoripples [34]. It is found that ripples or wrinkles act as potential barriers for charged carriers leading to their localization [35]. This fact confirms our findings (see Sec.IIIA) and serves as a solid argument in a favour of the vitality of our model. Indeed, it is observed that the potential surface variations are of around of 20-30 meV. In our model the ripple of the radius  $R = 12\text{\AA}$  yields the energy difference between the flat and curved graphene pieces  $\Delta\varepsilon \approx 24\text{meV}$  (see Eq.20). The THz time-domain spectroscopy may be used to provide contact-less, highly accurate information on conducting properties of the curved graphene surface (for a review see Ref.[36]), discussed in our paper.

Our analysis of the hybrid system that consists of the rippled +semiripple+flat pieces demonstrates the strong selectivity effect of transmitted electron trajectories. The ballistic electron transmission [see Eq.(41)] depends on the radius of the ripple, on the length of the arc of the ripple and on the width of the flat region between ripples. In fact, our system yields the higher selectivity in contrast to the one produced by the smooth step interface



(see Fig.6). Most important, that the superlattice, described in the paper, enables to one to control the conductance without *any additional electrical or magnetic sources*. Namely, the selectivity is controlled by the number of suitable  $N$  elements of the superlattice. The larger is the number of elements  $N$ , the stronger is the selectivity. At  $N \gg 1$ , only for the direction perpendicular to the surface of the  $\mathcal{S}$  subsystem there is almost the ideal transmission, while for the other angles ( $k_y \neq 0$ ) there is the strong reflection. This phenomenon is due to the Klein tunneling that is grown in our system by virtue of controlled graphene surface curvature.

### Acknowledgments

The work was supported in part by Slovak Grant Agency VEGA Grant 2/0009/19.

### Appendix A: The smooth potential step

The transmisson (47)

$$T(k_y) = \left[ \sinh \left( \pi k_F \ell \sqrt{1 - \left( \frac{k_y}{k_F} \right)^2} \right) / \sinh \pi k_F \ell \right]^2 \quad (\text{A1})$$

can be expressed in the limit  $k_F \ell \gg 1$  as

$$T(k_y) \approx \left[ \exp \left( \pi k_F \ell \sqrt{1 - \left( \frac{k_y}{k_F} \right)^2} \right) / \exp \pi k_F \ell \right]^2. \quad (\text{A2})$$

Assuming that nonzero transmission probabilities  $T(k_y) \neq 0$  exist only at the condition  $k_y/k_F \ll 1$ , we have finally

$$T(k_y) \approx \left[ \exp \pi k_F \ell \left( 1 - \frac{1}{2} \left( \frac{k_y}{k_F} \right)^2 \right) / \exp \pi k_F \ell \right]^2 \approx \exp \left[ -\pi k_F \ell \left( \frac{k_y}{k_F} \right)^2 \right], \quad (\text{A3})$$

which is the formula (48).

In the opposite limit  $k_F \ell \ll 1$ , the transmission (47) yields the expression

$$T(k_y) \approx \left[ \frac{\pi k_F \ell \sqrt{1 - \left( \frac{k_y}{k_F} \right)^2}}{\pi k_F \ell} \right]^2, \quad (\text{A4})$$

where it was used the approximation  $\sinh \alpha \approx \alpha$  for  $\alpha \ll 1$ . As a result we obtain

$$T(k_y) \approx 1 - \left( \frac{k_y}{k_F} \right)^2 = \cos^2 \varphi. \quad (\text{A5})$$


---

- [1] Ando T J 2005 *J. Phys. Soc. Jpn.* **74** 777.
- [2] Novoselov K S, Geim A K, Morozov S V, Jiang D, Katsnelson M I, Grigorieva I V, Dubonos S V and Firsov A A 2005 *Nature* **438** 197.
- [3] Zhang Y, Tan Y-W, Stormer H and Kim P 2005 *Nature* **438** 201.
- [4] Katsnelson M I, Novoselov K S and Geim A K 2006 *Nat. Phys.* **2** 620.
- [5] Cheianov V V and Fal'ko V I 2006 *Phys. Rev. B* **74** 041403(R).
- [6] Cheianov V V, Fal'ko V I and Altshuler B L 2007 *Science* **315** 1252.
- [7] Huard B, Sulpizio J A, Stander N, Todd K, Yang B and Goldhaber-Gordon D 2007 *Phys. Rev. Lett.* **98** 236803.
- [8] Sutar S, Comfort E S, Liu J, Taniguchi T, Watanabe K and Lee J U 2012 *Nano Letts.* **12** 4460.
- [9] Chen S, Han Z, Elahi M M, Habib K M M, Wang L, Wen B, Gao Y, Taniguchi T, Watanabe K, Hone J, Ghosh A W and Dean C R 2016 *Science* **353** (6307) 1522.
- [10] Klein O 1929 *Z. Phys. A: Hadr. Nucl.* **53** 157.
- [11] Wang K, Elahi M M, Wang L, Habib K M M, Taniguchi T, Watanabe K, Hone J, Ghosh A W, Lee G-H and Kim P 2019 *PNAS* **116** (14) 6575.
- [12] Kumar S and Parks D M 2015 *Nano Letts.* **15** 1503.
- [13] Baimova J A, Dmitriev S V, Zhou K and Savin A V 2012 *Phys. Rev. B* **86** 035427.
- [14] Liu B, Reddy C D, Jiang J, Baimova J A, Dmitriev S V, Nazarov A A and Zhou K 2012 *Appl. Phys. Lett.* **101** 211909.
- [15] de Juan F, Cortijo A and Vozmediano M A H 2007 *Phys. Rev. B* **76** 165409.
- [16] Katsnelson M and Geim A 2008 *Philos. Trans. R. Soc. A* **366** 195.
- [17] Guinea F, Katsnelson M I and Vozmediano M A H 2008 *Phys. Rev. B* **77** 075422.
- [18] Allain P E and Fuchs J N 2011 *Eur. Phys. J. B* **83** 301.
- [19] Pereira J M Jr, Peeters F M, Chaves A and Farias G A 2010 *Semicond. Sci. Technol.* **25** 033002.

- [20] Pudlak M, Pichugin K N and Nazmitdinov R G 2015 *Phys. Rev. B* **92** 205432.
- [21] Ando T 2000 *J.Phys. Soc. Jpn.* **69** 1757.
- [22] Pichugin K N, Pudlak M and Nazmitdinov R G 2014 *Eur. Phys. J. B* **87** 124.
- [23] Wei Y, Wang B, Wu J, Yang R and Dunn M L 2013 *Nano Lett.* **13** 26.
- [24] Bai Ke-Ke, Zhou Yu, Zheng H, Meng L, Peng H, Liu Z, Nie J-C and He L 2014 *Phys. Rev. Lett.* **113** 086102.
- [25] Low T, Hong S, Appenzeller J, Datta S and Lundstrom M S 2009 *IEEE Trans. Elec. Dev.* **56** (6) 1292
- [26] Pudlak M and Pincak R 2009 *Eur. Phys. J. B* **67** 565.
- [27] Pudlak M and Pincak R 2009 *Phys. Rev. A* **79** 033202.
- [28] Saito R, Dresselhaus G and Dresselhaus M S 2003 *Physical Properties of Carbon Nanotubes* (London: Imperial College Press).
- [29] Lomer W M 1955 *Proc. Roy. Soc. A* **227** 330.
- [30] Yaniv A 1978 *Phys. Rev. B* **17** 3904.
- [31] Wallace P R 1947 *Phys. Rev.* **71** 622.
- [32] Flügge S 1994 *Practical Quantum Mechanics* (Heidelberg: Springer-Verlag).
- [33] Alyobi M M M, Barnett C J, Rees P and Cobley R J 2019 *Carbon* **143** 762.
- [34] Ni G-X, Zheng Yi, Bae S, Kim H R, Pachoud A, Kim Y S, Tan C-L, Im D, Ahn J-H, Hong B H and Özyilmaz B 2012 *ACS Nano* **6** 1158.
- [35] Vasić B, Zurutuza A and Gajić R 2016 *Carbon* **102** 304.
- [36] Bøggild P, Mackenzie D M A, Whelan P R, Petersen D H, Buron J D, Zurutuza A, Gallop J, Hao L and Jepsen P U 2017 *2D Mater.* **4** 042003.

